ADAPTIVE GRID METHODS FOR NUMERICAL WEATHER PREDICTION

William C. Skamarock
National Center for Atmospheric Research *
Boulder, CO, USA

1. INTRODUCTION

The increasing speed and memory of supercomputers is allowing explicit resolution of a larger range of scales of atmospheric motion in a single computation. This can be seen most clearly in the global forecast models that are now being run regularly with spatial resolution of order 100 km. Atmospheric motions of interest, though, span many more scales than it is possible to explicitly capture in a single computation. Nonhydrostatic motions may contain significant features on scales ranging from several meters to several tens of kilometers with time scales of minutes to many hours. Hydrostatic motions, in which the nonhydrostatic motions are embedded, have motion scales orders of magnitude larger than the nonhydrostatic motions. The inability to explicitly resolve this large range of motion scales in numerical models has hindered both atmospheric research and numerical weather prediction.

Most weather phenomena are local in nature, however numerical models typically have uniform resolution everywhere. Adaptive numerical methods attempt to change resolution locally in response to the evolving solution. While adaptive numerical techniques have yet to be extensively applied in atmospheric models, we believe that the next generation of meso-scale/cloudscale models will be nonhydrostatic and will incorporate more sophisticated nested and adaptive grid techniques. In particular, these models should be suitable for studying scale interactions between nonhydrostatic and hydrostatic motions and may be suitable for limited NWP tasks after sufficient development. The purpose of this paper is to review the adaptive solution techniques that have been or can be applied in atmospheric models.

In general, the methods can be grouped into two general classifications; *global* and *local* refinement techniques. The global methods involve redistributing existing gridpoints in such a way that they become clustered in regions where the solution error is high. However, while the gridpoints move over time the methods are not Lagrangian because the gridpoints do not move with the fluid velocity. Gridpoint positions are determined each timestep using a *grid generation* technique and the gridpoint velocities are the difference in the gridpoint locations divided by the timestep. Several variants of this general technique will be discussed in Section

* The National Center for Atmospheric Research is supported by the National Science Foundation

2 and two adaptive computations of atmospheric flow using a global refinement technique are presented.

Local methods adaptively refine the solution by adding points where the solution error is high. Two variants of this technique exists. The first adds gridpoints to an existing grid, usually by subdividing grid cells. While this technique has been used for time-dependent problems in engineering applications, the author knows of no atmospheric models based on this approach. The second class of local refinement methods makes use of separate fine grids which overlie existing coarser grids. The collection of grids interact in the same manner as the two-way interactive nested grids that are popular in atmospheric models. The local refinement techniques will be discussed in Section 3. Two and three-dimensional nonhydrostatic adaptive simulations using nested grids are given at the end of the section.

2. GLOBAL REFINEMENT METHODS

In this section we briefly discuss global refinement methods and show some simple numerical examples. An excellent general review of the methods is presented by Hawken *et al* 1991 and more specialized reviews are given in Anderson (1983), Thompson (1985) and Eiseman (1987). A large portion of the development of these methods has taken place in the aerodynamics community and this work is highlighted in these reviews.

Global refinement techniques involve moving gridpoints automatically such that they are clustered in regions where the solution error is high. The methods consist of two components. First, an algorithm is needed for solving the set of governing equations transformed from physical space, where the grid is nonuniform, possibly nonorthogonal and in motion, to computational space where the grid is regular and stationary. Second, a *grid generation* algorithm must be used to compute new gridpoint locations. The most popular grid generation methods, which seek to minimize or equidistribute some measure of the solution error, involve solving a set of elliptic equations that are derived from a combination of variational problems that, in addition to equidistributing the error, attempt to maintain some grid properties such as orthogonality or grid smoothness.

Three general styles of moving gridpoint methods exists. Periodic gridpoint-movement methods hold the gridpoints fixed in physical space for several timesteps after which they are

shifted to new positions. Typically data is moved from the old to the new grid using some interpolation scheme. The PDEs do not contain terms pertaining to gridpoint movement. Alternating gridpoint-movement methods require that the gridpoints be moved after every timestep with data being transferred using interpolation. Again, gridpoint movement does not appear in the PDEs. Finally, simultaneous gridpoint-movement methods move the gridpoints and integrate the PDEs simultaneously. Thus the dynamical PDEs contain terms for the gridpoint velocities. No interpolation is required with this method.

The periodic and alternating gridpoint-movement methods can result in a mismatch of gridpoint distribution and solution, and suffer from instabilities and oscillations if timesteps are too large. Also, interpolations can be difficult to design, particularly when it is necessary to conserve certain fluid properties. Thus the periodic and alternating gridpoint-movement methods appear unsuitable for meteorological problems. In this paper we will review the simultaneous gridpoint-movement methods. Note, however, that the simultaneous gridpoint-movement methods are the most complex.

The global refinement techniques offer one major advantage over most local refinement techniques – the transition between regions of high resolution and low resolution is smooth. This feature removes some of the wave reflection and wave dispersion problems that are common in local refinement methods where points are added to a regular grid or where nested fine grids are used. Although this feature is highly desirable, the global methods also have several undesirable features. First, the grid is no longer regular. The transformation to computational space produces numerous additional terms that need evaluation and, of course, the grid metrics must be recomputed each timestep. The grid must be generated anew each timestep, most often by solving a set of elliptic equations. In time dependent problems where the equations are integrated with explicit methods, the time step is limited by the stable timestep for the smallest grid volume. Increasing the resolution in one region reduces resolution in another, and it is only by adding points that a given overall solution accuracy can be guaranteed. Finally, in atmospheric models, it is not clear how to correctly incorporate parameterizations that are dependent in the gridscale. While this problem is also present in nested models, the parameterizations pose a greater problem on the non-regular grids because the gridscale changes dramatically on the single grid.

2.1 Continuous Dynamic Grid Adaption

In this section we outline the efforts of Dietachmeyer and Droegemeier (DD, 1991) and Dietachmeyer (1991) who construct simple atmospheric models based on a simultaneous gridpoint-movement method which they denote *Dynamic Grid Adaption*. First we give an example of the equations written in terms of curvilinear coordinates with the gridpoint movement terms included, followed by a description of two grid-generation algorithms used by DD and Dietachmeyer. After a brief description of the overall solution sequence, three computational examples are given. To the authors knowledge, DD represents the first attempt to use moving-gridpoint adaptive methods in atmospheric models.

To illustrate the basic technique, consider the two-dimensional advection equation

$$\frac{\partial \phi}{\partial t} = -u\frac{\partial \phi}{\partial x} - v\frac{\partial \phi}{\partial y} \tag{1}$$

First we need to recast (1) into the $(\varepsilon, \eta, \tau)$ coordinate system with $x(\varepsilon, \eta, \tau)$, $y(\varepsilon, \eta, \tau)$ and $t = \tau$. Using the chain rule we can restate (1) as

$$\frac{\partial \phi}{\partial \tau} = (\dot{x} - u)\frac{\partial \phi}{\partial x} + (\dot{y} - v)\frac{\partial \phi}{\partial y}, \tag{2}$$

where $\dot{x}$ and $\dot{y}$ are the velocities of the gridpoints. The fully transformed equations can be expressed with the aid of the Jacobian of the transformation

$$G^{1/2} = \frac{\partial x}{\partial \varepsilon}\frac{\partial y}{\partial \eta} - \frac{\partial x}{\partial \eta}\frac{\partial y}{\partial \varepsilon}$$

as

$$\frac{\partial \phi}{\partial \tau} = -\frac{1}{G^{1/2}}\left((u - \dot{x})\frac{\partial y}{\partial \varepsilon} + (v - \dot{y})\frac{\partial x}{\partial \eta}\right)\frac{\partial \phi}{\partial \varepsilon} - \frac{1}{G^{1/2}}\left((v - \dot{y})\frac{\partial x}{\partial \eta} + (u - \dot{x})\frac{\partial y}{\partial \varepsilon}\right)\frac{\partial \phi}{\partial \eta}, \tag{3}$$

i.e.

$$\frac{\partial \phi}{\partial \tau} = -\mathrm{ueff}\frac{\partial \phi}{\partial \varepsilon} - \mathrm{v_{eff}}\frac{\partial \phi}{\partial \eta}. \tag{4}$$

Before considering the grid-generation algorithms, note that while we have transformed the independent variables x, y and t, we have retained the cartesian velocities u and v. This is a convenient, though not necessary choice. Transforming of the velocities would lead to the addition of metric derivatives. Transformation of the nonlinear momentum equations does not introduce any increased complexity, although second derivative terms are increasingly tedious to evaluate. For example, a second derivative term ϕ_{xx} would be transformed into

$$\begin{aligned}\phi_{xx} = {} & G^{-1}(y_\eta^2\phi_{\varepsilon\varepsilon} - 2y_\varepsilon\phi_{\eta\varepsilon} + y_\varepsilon^2\phi_{\eta\eta}) \\ & + a_1(x_\eta\phi_\varepsilon - x_\varepsilon\phi_\eta) + a_2(y_\varepsilon\phi_\eta - y_\eta\phi_\varepsilon)\end{aligned}$$

where

$$a_1 = G^{-3/2}(y_\eta^2 y_{\varepsilon\varepsilon} - 2y_\varepsilon y_\eta y_{\eta\varepsilon} + y_\varepsilon^2 y_{\eta\eta}),$$
$$a_2 = G^{-3/2}(y_\eta^2 x_{\varepsilon\varepsilon} - 2y_\varepsilon y_\eta x_{\eta\varepsilon} + y_\varepsilon^2 x_{\eta\eta}).$$

For a prognostic equation set, the evaluation of this term is tedious but not problematic. However, an elliptic equation posed in curvilinear coordinates will be difficult to invert.

The grid generators determine the gridpoint locations (x,y) as a function of (ε,η) given some measure of the solution error. A large variety of grid-generation methods exist. and they can be subdivided into four groups; elliptic, parabolic, hyperbolic and algebraic grid generators. The names reveal the types of equations that must be solved to generate the grids. We outline an elliptic and an algebraic grid generation method used by Dietachmeyer and Droegemeier (1991) and Dietachmeyer (1991).

Both grid generation schemes seek to equidistribute a measure of the solution gradient and curvature W. For example in DD

$$W(x,y,t) = (1 + \alpha_2|\kappa|)[1 + \alpha_1|\nabla\phi|^2]^{1/2} - 1, \tag{5}$$

where α_1 and α_2 are arbitrary coefficients, ϕ is the dependent variable and κ is the curvature defined as

$$\kappa = \frac{|\nabla^2\phi|}{[1 + |\nabla\phi^2|]^3}.$$

The elliptic grid generator used by DD is based on the algorithm of Brackbill and Saltzman (1982). It is most clearly described as a technique that minimizes the weighted integral measures of smoothness, orthogonality and adaptivity. This integral can be expressed as

$$\begin{aligned} I &= I_s + \lambda_o I_o + \lambda_W I_W \\ &= \iint \left(G + \lambda_o G_{12}^2 + \lambda_W G W^2\right) d\varepsilon d\eta \end{aligned} \tag{6}$$

where λ_o and λ_W are free parameters and G_{ij} are the components of the conjugate tensor of the transformation (see Gal-Chen and Somerville, 1975). The next step is to recast the minimization of I into a set of coupled elliptic equations. Defining $F = g(1 + \lambda_W^2) + \lambda_o g_{12}^2$,

the resulting elliptic set is

$$\sum_{i=1}^{2}\sum_{j=1}^{2}\left[\left(\frac{\partial F}{\partial G_{ij}}+\frac{\partial F}{\partial G_{ji}}\right)\frac{\partial^2 x_l}{\partial\varepsilon^i\varepsilon^j}+\frac{\partial x_k}{\partial\varepsilon^j}\frac{\partial}{\partial W}\left(\frac{\partial F}{\partial G_{ij}}+\frac{\partial F}{\partial G_{ji}}\right)\sum_{m=1}^{2}\frac{\partial W}{\partial x_m}\frac{\partial x_m}{\partial\varepsilon^i}+\right.$$
$$\left.\frac{\partial x_k}{\partial\varepsilon^j}\sum_{m=1}^{2}\sum_{n=1}^{2}\left\{\left(\frac{\partial}{\partial G_{mn}}\frac{\partial F}{\partial G_{ij}}+\frac{\partial F}{\partial G_{ji}}\right)\sum_{p=1}^{2}\left(\frac{\partial^2 x_p}{\partial\varepsilon^m\partial\varepsilon^i}\frac{\partial x_p}{\partial\varepsilon^n}+\frac{\partial^2 x_p}{\partial\varepsilon^m\partial\varepsilon^n}\frac{\partial x_p}{\partial\varepsilon^i}\right)\right\}\right]$$
$$-\frac{\partial F}{\partial W}\frac{\partial W}{\partial x_l}=0 \qquad \text{for} \quad l=1,2 \tag{7}$$

The coupled equations (7) along with the appropriate boundary conditions can be solved iteratively (DD, Brackbill and Saltzman 1982). However, the solution of the coupled set can be very expensive relative to the solution of the governing PDEs. DD do not discuss in detail the efficiency of their scheme, though they note that it is very expensive and that alternate grid generation algorithms need to be developed in order to make the moving gridpoint methods attractive for atmospheric integrations.

In a later work, Dietachmeyer (1991) presents a new algebraic grid generation scheme that is considerably less expensive than the previous elliptic grid-generation method. It is based on the observation that the equidistribution of the error, which is approximated by the weight function (5) implies

$$W \cdot dA = \text{constant.}$$

In practice Dietachmeyer uses an equidistribution equation of the form

$$F \cdot dA = \text{constant.} \tag{8}$$

where $F = (1 + \lambda_W W)$. Dietachmeyer outlines an iterative procedure which leads to the solution of a discretized form of (8). The method involves adjusting each gridpoint location in turn such that the four adjacent gridcells more closely satisfy (8) and the constant is determined as part of the solution method. The algorithm, which appears similar to traditional relaxation methods for elliptic PDEs, makes use of two boundary conditions; the boundary points must lie on the physical boundary and the grid must be orthogonal at the boundary. Convergence rates for the method are very good and the efficiency of the new grid-generation technique suggests that the 2-D moving-gridpoint adaptive method is economically feasible for use in many atmospheric calculations.

Dietachmeyer's algebraic grid generation method does not possess the constraints on smoothness and orthogonality that are incorporated into the Brackbill-Saltzman grid generation scheme (see eq. 6). Grid smoothness is desired, for nonsmooth grids can lead to increased truncation error. Dietachmeyer demonstrates that by filtering the weight function using a (1 2 1) filter the desired grid smoothness is achieved. Sufficiently smooth weight functions will lead to sufficiently smooth grids using this method.

Dietachmeyer further increases the efficiency of the method by updating the gridpoint velocities only after every several timesteps, between the update the gridpoint velocities are held fixed. This method retains the advantages of the simultaneous gridpoint-movement methods while decreasing the overall cost of the method by calling the grid generator less frequently. In some simple test cases it was found that there could be as many as 10+ timesteps between grid generations.

There are several methods used to couple the PDE integration and the grid generation in the moving-gridpoint schemes. The most complex approaches couple the two systems together by requiring that the gridpoint locations $x(\varepsilon, \eta, \tau + \Delta\tau)$ and $y(\varepsilon, \eta, \tau + \Delta\tau)$ be dependant on the solution $\phi(\varepsilon, \eta, \tau + \Delta\tau)$, i.e., the weight function used in the grid generation scheme for determining the gridpoint locations at time $\tau + \Delta\tau$ is a function of the solution at $\tau + \Delta\tau$. DD use a simpler approach in which x and y at $\tau + \Delta\tau$ are only dependent on the solution at time τ. Thus the grid generation and the PDE integration are not explicitly coupled in the timestep.

Given the solver for the governing equations posed in curvilinear coordinates and the grid-generation algorithm, the solution procedure used by DD is as follows. First, using the solution at time τ, the grid generation is performed with the weighting function W evaluated using the solution at time τ. The resulting gridpoint locations are for time $\tau + \Delta\tau$ and the gridpoint velocities are defined as $\dot{x}_i = (x_i^{\tau+\Delta\tau} - x_i^{\tau})/\Delta\tau$. Then, the governing PDE is integrated using whatever method is desired. It should be noted that the timestep is often limited by the gridscale of the smallest gridcell. In most moving gridpoint models, the timestep size is adjusted after every timestep to maintain the stability of the integrations. Multiple-time-level integration schemes are not often used in these applications because of the changing timesteps. DD and Dietachmeyer use the modified Heun method.

Three examples of the DD dynamic grid adaption are given here. The first example is the 2-D kinematic frontogenesis case discussed by Davies-Jones (1985).

Equation (1) is solved with the initial condition

$$\phi(x,y,0) = -\tanh(y/2)$$

where the radially symmetric, time invariant wind field is given by

$$v_{tangential} = \operatorname{sech}^2 r \tanh r.$$

The initial conditions for ϕ along with the flow field is given in Figure 1a. Figure 1b shows the exact solution at a given time, Figure 1c shows the solution at that time on a fixed grid with 31 × 31 points and Figure 1d depicts the adaptive solution on a grid using the same number of gridpoints as the fixed grid. The adaptive grid at the final time is shown in Figure 1e. The solution on the fixed grid contains spurious overshoots and undershoots along the spiral arms because the sharp gradients in ϕ are not resolved. A fixed grid with nearly double the spatial resolution (not shown) will give nearly the exact solution. The adaptive solution resolves the high-gradient regions of ϕ much better than the fixed coarse grid solution. In the adaptive solution the gridpoints are clustered about the center of the domain. Note that it is not possible to discern the individual arms in the grid response. Higher resolution adaptive runs show that the grid generator will produce grids which discern the arms when a sufficient number of gridpoints exist.

In the previous example the gridpoints are clustered in the center of the domain and the phenomena doesn't move. Next DD simulate a dry thermal. The governing equations used for the thermal are in streamfunction–vorticity form and can be expressed as

$$\psi_t = -u\psi_x - w\psi_z - (g/\theta_o)\theta'_x + \nu\nabla^2\psi$$
$$\theta'_t = -u\theta'_x - w\theta'_z + \nu\nabla^2\theta'$$

where

$$\psi = u_x - w_z = \nabla^2\phi.$$

Subscripts denote differentiation in these equations and θ' is the potential temperature perturbation from a constant reference state θ_o. The transformation to the computational coordinates (ε, η) is given in DD.

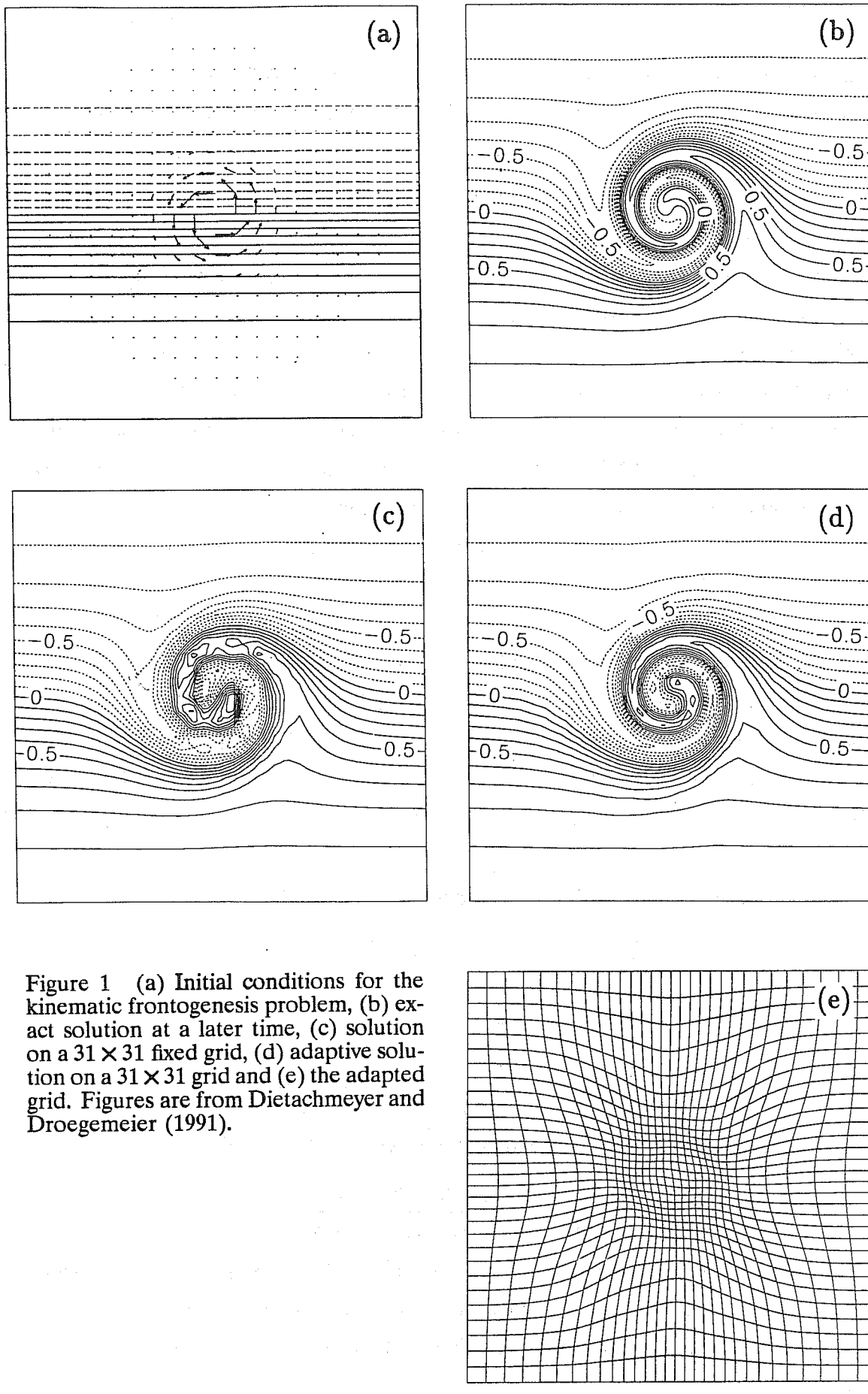

Figure 1 (a) Initial conditions for the kinematic frontogenesis problem, (b) exact solution at a later time, (c) solution on a 31×31 fixed grid, (d) adaptive solution on a 31×31 grid and (e) the adapted grid. Figures are from Dietachmeyer and Droegemeier (1991).

The initial conditions for their simulations consist of a warm bubble in a quiescent atmosphere. These conditions are depicted in Figure 2a. The enclosed domain is 800m in width and 1000m in height and the warm bubble has a maximum perturbation of .5*K*. In this simulation a 2 m^2s^{-1} viscosity is used and is chosen so as to limit the sharpness of the interface between the rising thermal and its environment. Figure 2b shows a fine grid solution (61 × 61 points) at 15 minutes, Figure 2c shows a coarse grid solution (31 × 31 points) at the same time, Figure 2d depicts the adaptive solution with 31 × 31 points at this time with the corresponding adaptive grid given in Figure 2e. Examination of the fixed grid solution reveal spurious extrema on the central axis at this time. Spurious extrema also exists off axis at earlier times but are damped by viscosity. The interior of the thermal is also extremely ragged and the leading edge is smeared. The adaptive solution contain none of these deficiencies. There is high resolution along the arms of the thermal but relatively low resolution in the thermal interior. DD speculate that the adaptive gridding resolves the thermals sufficiently well that downstream oscillations are not generated.

The previous examples used the Brackbill-Saltzman grid generation algorithms. In the next example, the algebraic grid generation algorithm of Dietachmeyer is used in an adaptive simulation of multiple barotropic eddies. The multiple eddies require that the adaptive grid respond to several discontinuous, separate features as opposed to the single continuous solution features needing refinement in the previous examples.

Dietachmeyer integrates the shallow water equations on a sphere.

$$\begin{aligned}
\frac{du}{dt} &= -\frac{1}{a\cos\theta}\frac{\partial\phi}{\partial\lambda} + \left(f + \frac{u\tan\theta}{a}\right)v \\
\frac{dv}{dt} &= -\frac{1}{a}\frac{\partial\phi}{\partial\theta} - \left(f + \frac{u\tan\theta}{a}\right)u \\
\frac{d\phi}{dt} &= -\phi\left[\frac{1}{a\cos\theta}\frac{\partial u}{\partial\lambda} + \frac{1}{a\cos\theta}\frac{\partial(v\cos\theta)}{\partial\lambda}\right]
\end{aligned}$$

where λ and θ are the longitude and latitude respectively, a is the radius of the earth and

$$\frac{d}{dt} = \frac{\partial}{\partial t} + \frac{u}{a\cos\theta}\frac{\partial}{\partial\lambda} + \frac{v}{a}\frac{\partial}{\partial\theta}$$

Figure 3a and b show the height field and adaptive grid at a single time in an adaptive calculation of three vortices. The domain varies longitudinally from 0^o to 55^o and latitudinally from -5^o to -55^o (southern hemisphere). The vortices are well space and the grid deforms

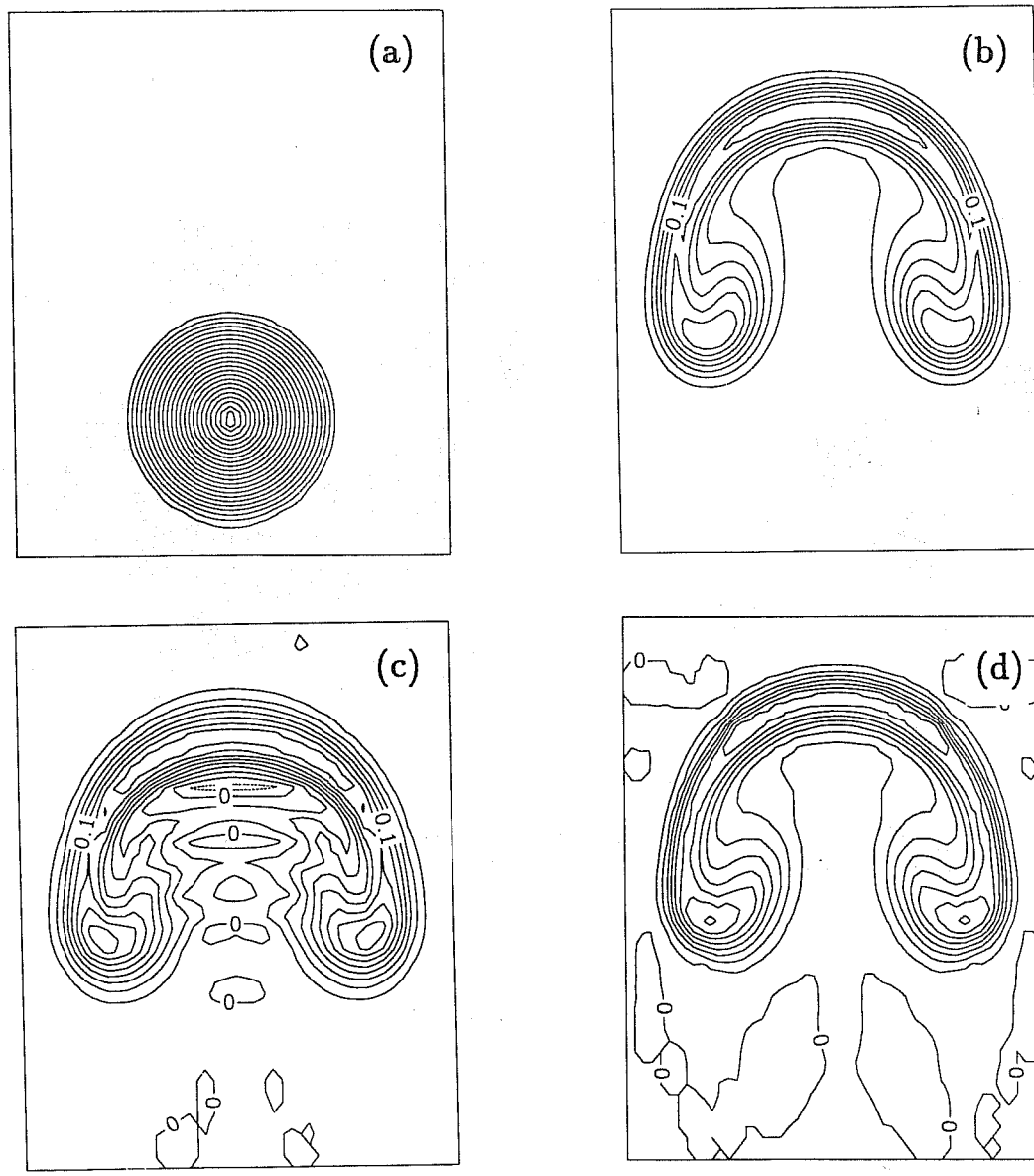

Figure 2 (a) Initial θ field for the buoyant thermal, (b) θ at 15 minutes on a 61×61 fixed grid, (c) on a 31×31 fixed grid, (d) adaptive solution on a 31×31 grid and (e) the adapted grid. Figures are from Dietachmeyer and Droegemeier (1991).

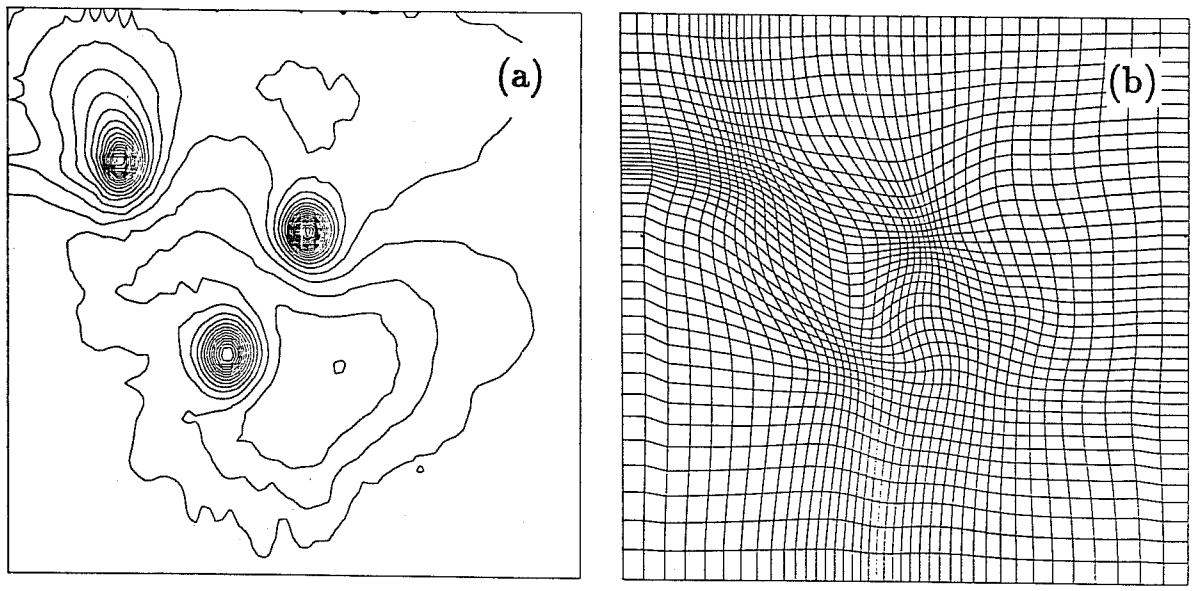

Figure 3 (a) Height field at a later time in an barotropic adaptive simulation and (b) the adapted grid. Figures are from Dietachmeyer (1991).

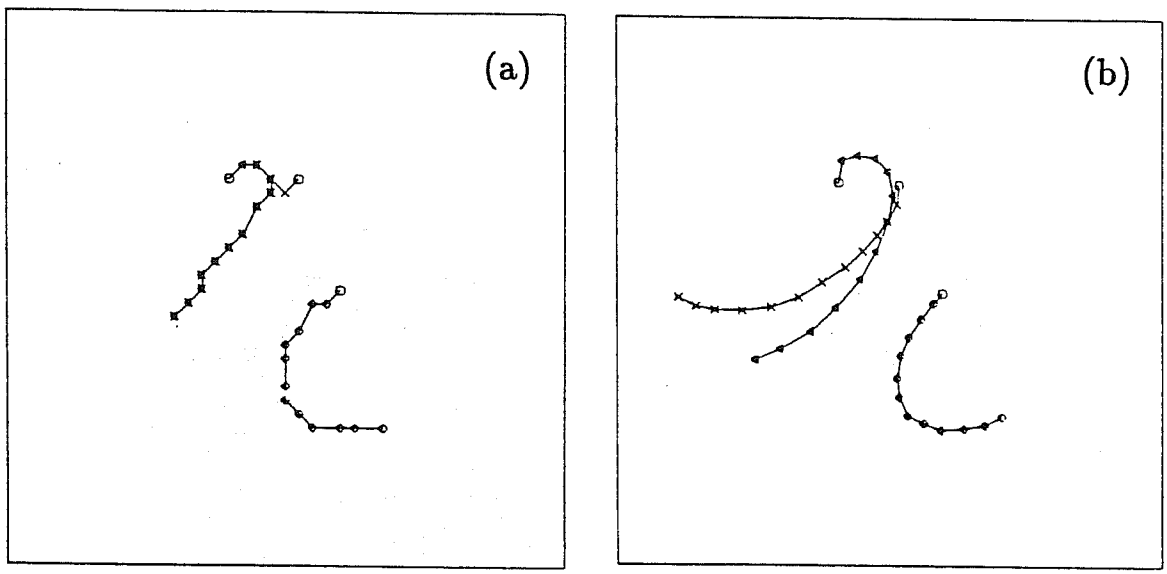

Figure 4 Cyclone tracks for (a) a fixed coarse grid and (b) for a fixed fine grid. Only on the coarse grid do the vortices merge. Figures are from Dietachmeyer (1991).

in such a way as to cluster points about the vortices. When the vortices are well spaced the cyclone tracks are well predicted even on a fixed coarse grid, however, the amplitude is poorly predicted. When cyclones are closely spaced the fixed coarse grid does not even predict the track well while the adaptive model does produce accurate tracks (here the exact solution is that obtained on a very fine fixed grid). Cyclone tracks for a fixed coarse grid, adaptive and fixed fine grid are given in Figure 4. Note that in the coarse grid two of the original three cyclones merge, while in the adaptive solution with the same number of gridpoints the cyclones do not merge.

Using the algebraic grid generator, Dietachmeyer finds that the adaptive calculations are a few to several times less expensive than fixed grid simulations which give solution of similar accuracy. As noted earlier, use of the Brackbill-Saltzman grid generator results in integration times much greater than the comparable fixed grid simulations (in some case being two orders of magnitude greater). While more complex equation sets will help amortize some of the grid generation costs, the use of an efficient grid generator is crucial to the cost effectiveness of the scheme.

Finally, we reiterate that work on the moving gridpoint adaptive methods is still progressing. It is not clear how to incorporate some of the standard parameterizations that depend on gridscale into the scheme given that the grid changes continuously. The equation sets grow very complex when higher order derivatives are approximated on the nonorthogonal grid. Also, extension to three dimensions may prove extremely difficult because of the much more complex transformed equation sets and more difficult still is the grid generation task in three dimensions. At this point, it appears that moving gridpoints methods are feasible in two dimensions.

3. LOCAL REFINEMENT METHODS

3.1 Grid-Cell Subdivision

Local refinement methods that involve adding gridpoints or dividing grid cells have been exploited by many modellers. In this approach there is only one grid, and gridpoints are added to the grid where necessary by subdividing gridcells or elements. The irregularity of the grid gives rise to a complex solution algorithm and prevents the use of standard solvers. The primary advantage possessed by these techniques is that refinement can be more easily

tailored to the phenomena; fewer gridpoints need to be used. We know of no efforts to construct atmospheric models using this approaches.

There are examples of adaptive time-dependent Navier Stokes integrations in the aerodynamic community using a grid-cell subdivision method. Kallinderis and Baron (1989) add gridpoints to a grid in an evolving transonic flow calculation by means of subdividing gridcells with the solution being calculated using a finite-volume numerical method. A calculation of transonic flow over an airfoil is given in Figure 5a along with the adaptive grid in Figure 5b. In this calculation the Navier-Stokes equations are integrated in the appreciably viscous regions while the inviscid Euler equations are integrated in the rest of the domain. The adaptive algorithm, which make use of an expert system to determine refinement location, resolves well the shocks and the boundary layer on the airfoil. However, note that the grid is complex. Standard solvers can no longer be used and because of the highly irregular grids these solution techniques have not been widely used for fluid flow calculations.

3.2 Adaptive Mesh Refinement

In this section we outline the Adaptive Mesh Refinement technique (AMR) of Berger and Oliger (1984). The adaptive method involves nesting fine grids based on refinement criteria extracted from the evolving solution. It generalizes the nesting procedures often used in other atmospheric models by allowing multiple, overlapping and arbitrarily oriented grids on any refinement level. AMR has been successfully used for many fluid flow problems including large-scale hydrostatic atmospheric flows (Skamarock et al, 1989), transonic airflow (Berger and Jameson 1985, Berger and Colella 1989) and steady-state and time-dependent Navier-Stokes equations (Caruso et al 1986, Thompson and Ferziger 1989, Perng 1990). AMR is being used in nonhydrostatic models and adaptive nonhydrostatic simulations will be presented following a description of the method.

The adaptive solution procedure for hyperbolic systems begins with a coarse-grid solution valid at some time t. The numerical error (normally the truncation error) in the solution is estimated at the gridpoints. Where the error is greater than some predetermined tolerance the points are flagged indicating that the area needs refinement. Rectangles (the fine grids) are fit enclosing these points. The grids may overlap and they need not be aligned with the base grid. Initial conditions for the fine grids are interpolated from the coarse grid or possibly

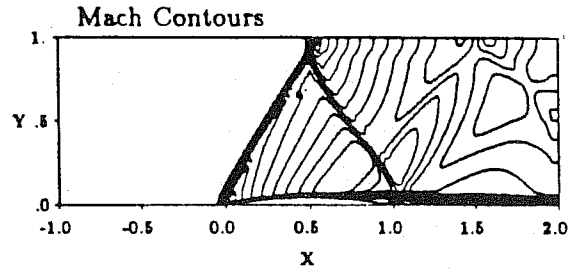

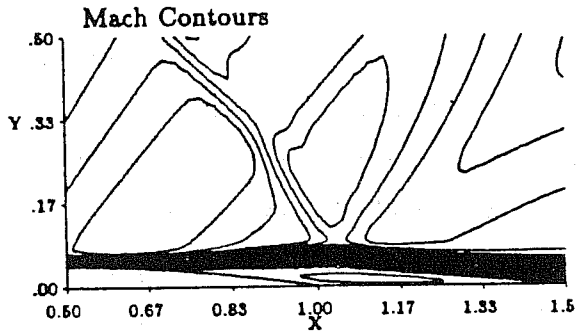

enlargement of shock/boundary layer interaction region

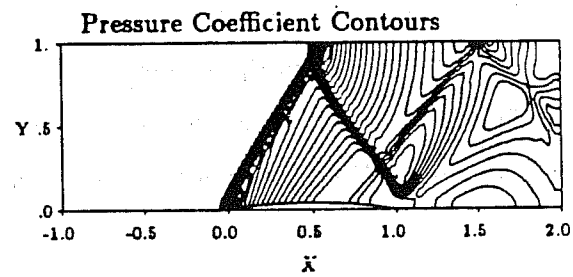

Figure 5 Mach number and pressure contours for supersonic flow past an 8% circular arc cascade. Figures are from Kallinderis and Baron (1989).

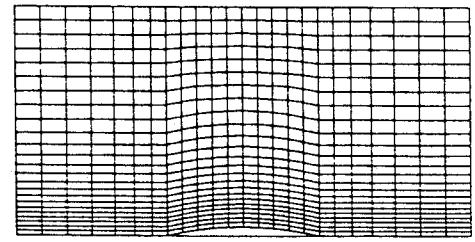

a) Initial grid (25 × 25)

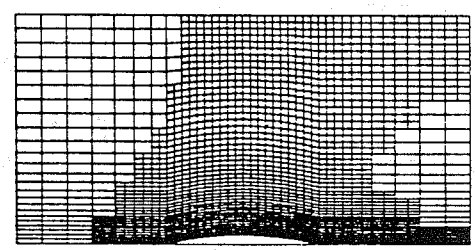

b) First embedding level

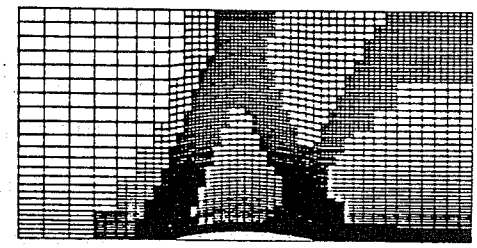

c) Second embedding level

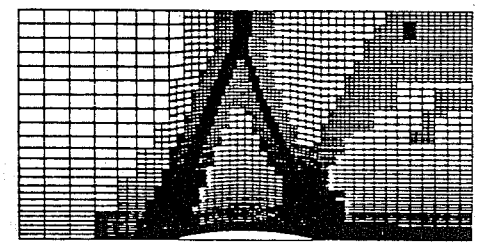

d) Third embedding level

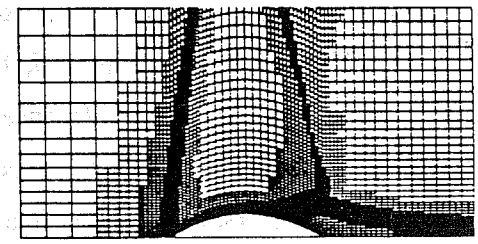

e) Third embedding level
(vertical scale enlarged)

Figure 6 Adaptive grid evolution Figures are from Kallinderis and Baron (1989).

from previously existing fine grids. Next, the coarse and fine grids are integrated from time t to time $t + \Delta t_{\text{coarse}}$. The time steps on the fine grids are smaller than those on the coarse grid so as to keep $\Delta x/\Delta t$ constant on the different grids (as is appropriate for hyperbolic systems). Fine-grid boundary values are interpolated, spatially and temporally, from the coarse grid or from the fine grids in places where fine grids overlap. When all grids have been integrated over the time step, the values at the coarse grid points that lie inside of a fine grid are replaced (updated) with an appropriately averaged value from the fine grids. This process may now be repeated for the next time step. The error estimate and recreation of the fine grids need not occur at each timestep but rather only at specified intervals. By periodically re-estimating the error and creating new fine grids, the grids can move with whatever is responsible for the high error, usually some prominent solution feature. A fully adaptive method is achieved by allowing for error estimation on the fine grids and the introduction of still finer grids.

AMR offers advantages over other adaptive approaches. All grids are regular, hence pre-existing fast solvers can be used. Any number of refinement levels can be invoked, hence the solution accuracy is not limited by the algorithm. Parameterizations can be tailored to the resolution of the particular grid, something that is difficult to do with the moving-gridpoint methods. AMR can be used with parallel and distributed solution techniques. The primary disadvantage is the existence of internal, fine-grid boundaries. Wave reflection is a problem where the resolution abruptly changes.

Before considering the details of the AMR approach, it is worthwhile to briefly consider the existing nested hydrostatic and nonhydrostatic models. The fine grids in AMR function as 2-way interactive nested grids commonly used in atmospheric models. Grid nesting has been used extensively in hydrostatic models. Examples in a research setting are the Penn State/NCAR MM4 model (Zhang *et al*, 1986) and in an operational setting the NGM used at NMC (Hoke *et al, 1990*). In both cases the grids are fixed in both number and location though recently the MM4 has incorporated the ability to have multiple fine grids that move in time (George Grell, personal communication). Applications where the fine grids are allowed to move include the hurricane models of Harrison (1973) and Jones (1977). These nested models are not truly adaptive in that it must be known a priori where increased resolution will be needed and how large the refined region must be.

There are fewer nested nonhydrostatic models. Clark and Farley (1984) constructed a nested model based on an anelastic set of equations. The system allows multiple nesting but they cannot be rotated with respect to the base grid and multiple overlapping grids cannot be used on the same refinement level. Solution of the elliptic pressure equation in the nested configuration does not appear to impose any significant computational penalty.

The nonhydrostatic AMR model uses a compressible equation set along with a split-explicit solution technique. This choice of equations and solution technique allows straightforward use of rotated, overlapping fine grids. Fine grid rotation is difficult to achieve when using the anelastic system, or any system in which exact mass conservation is important, because interpolations for boundary conditions and averaging for updating must be conservative. Hydrostatic nested and adaptive models generally have not used conservative interpolation and averaging procedures, examples being Skamarock et al (1989), Zhang *et al* (1986), Jones (1977), Harrison (1973) and others. The elastic nonhydrostatic system is similar to the hydrostatic system in that both have prognostic, hyperbolic equations for pressure and this suggests that strictly conservative interpolation and averaging procedures are not essential for the elastic model.

The remainder of this section outlines boundary condition specification for the interior fine grids, updating procedures, and presents examples of the nested/adaptive AMR simulations using a nonhydrostatic, elastic set of equations. Details of the error-estimate procedures are given in Skamarock (1989). Algorithmic details and data structures, along with a more general overview of AMR can be found in Berger and Oliger (1984).

The updating and boundary condition procedures used in the adaptive model are as follows. For updating coarse grid values that lie in a fine grid, the fine-grid values are averaged over an equivalent coarse-grid volume and then the new coarse-grid values are bilinearly interpolated from these averaged values. Interpolation is necessary when a fine grid is rotated with respect to a coarse grid because coarse and fine gridpoint locations may no longer coincide.

Boundary conditions are required for both the coarse and fine grids. The coarsest grid has its boundary conditions satisfied through some numerical representation of the physical boundary conditions. Fine grid boundary conditions consists of quadratic spatial and linear

temporal interpolation of all variables, except pressure, to the fine grid boundaries from the interior of the coarser grid(s). The interpolated variables include a velocity normal to the boundary and, one-half Δx_n inward from the boundary, a tangential velocity and all other variables. Boundary values for overlapping fine grids must be interpolated from the other fine grid where possible, while all other boundary value come from the coarser grids.

The solution procedure used in the nonhydrostatic AMR model is the split explicit technique described by Klemp and Wilhelmson (1978) with the addition of an acoustic filter discussed in Skamarock and Klemp (1991). The technique requires that several small timesteps be used to advance the acoustic modes within the leapfrog timestep used to integrate the non-acoustic modes. Proper transmission of soundwaves through boundaries would require that boundary value interpolations and updating occur every small timestep because the sound wave terms are integrated with the small timesteps. However, the soundwaves are meteorologically insignificant and the overhead associated with the updating and interpolations is not insignificant. Hence, boundary value interpolations and updating occur only every large timestep. Also note that the overlapping fine grids are independently integrated over a single timestep and boundary values for the small timesteps between t and $t + \Delta t$ are not yet available from the neighboring fine grid. In this case the boundary values needed on the small timestep between t and $t + \Delta t$ are linearly extrapolated using the boundary values at time t and $t - \Delta t$. The extrapolated values are replaced with the values interpolated from the overlapping fine grids after the full timestep is complete for both grids. Finally, we note that the discretized pressure equation needs no boundary conditions, its stencil is complete at all point on the grid. However, the boundary pressures are replaced with values interpolated from overlapping or coarser grids at the end of the leapfrog timestep so as to keep the pressure solutions on the various grids more closely coupled.

3.2.1 2-D Nonhydrostatic AMR Simulations

In this section adaptive results for two different flows are presented using the following dry, Boussinesq, elastic equation set. The Boussinesq, dry, adiabatic equations used in the 2-D model are

$$\frac{\partial u}{\partial t} + \frac{\partial \pi}{\partial x} = -u\frac{\partial u}{\partial x} - w\frac{\partial u}{\partial z} \tag{9}$$

$$\frac{\partial w}{\partial t} + \frac{\partial \pi}{\partial z} - g\left(\frac{\theta}{\bar{\theta}} - 1\right) = -u\frac{\partial w}{\partial x} - w\frac{\partial w}{\partial z} \tag{10}$$

$$\frac{\partial \pi}{\partial t} + c_s^2\left(\frac{\partial u}{\partial x} + \frac{\partial w}{\partial z}\right) = 0 \tag{11}$$

and

$$\frac{\partial \theta}{\partial t} + u\frac{\partial \theta}{\partial x} + w\frac{\partial \theta}{\partial z} = 0. \tag{12}$$

Equations (9)–(12) are the u and w-momentum, pressure and thermodynamic equations respectively. u and w are the fluid velocities in x and z, θ is the potential temperature and $\bar{\theta}(z)$ is the mean potential temperature, π is the perturbation Exner function ($\Pi = C_p\theta(p/p_o)^{R/C_p}$), g is the gravitational constant, t is time and c_s is the speed of sound. The sound speed is constant. As noted earlier, integration of (9)-(12) is performed with a time-split scheme where the terms responsible for the sound waves are separated from the remaining terms and integrated with a smaller timestep. Second order accurate, centered spatial discretization is used.

Both flows in the adaptive simulations result in horizontally propagating gravity currents, one starting from the release of a cold bubble in a closed box, and the other arising from the collapse of a cold pool (Skamarock and Klemp, 1989). In the first simulation the viscosity is fixed and a grid-independent solution is very nearly attained. However, in the second simulation the viscosity is a function of the resolution and the solution does not converge. This non-convergence has implications for the evaluation of any solution computed with adaptive, nested, and grid refinement models in which parameterizations are a function of the resolution.

In the first simulation all physical boundaries are solid, free-slip surfaces. The domain length is 24 km and its height is 12 km. The initial cold bubble is specified as follows:

$$\Delta\theta = \begin{cases} 0. & L \geq 1 \\ -15[\cos(\pi L) + 1]/2 & L \leq 1 \end{cases};$$

where

$$L = \left[\frac{(x - x_o)^2}{x_r^2} + \frac{(z - z_o)^2}{z_r^2}\right]^{\frac{1}{2}}$$

and $x_o = 0$, $x_r = 4000$m, $z_o = 3000$m, and $z_r = 2000$m. The initial velocities are zero and the initial pressure π is the anelastic pressure. The model parameters used in the runs are Δx_c, $\Delta z_c = 300$m, $\Delta t_c = 4.0$s, $\Delta\tau = 0.5$s, $\alpha = 0.05$ and $\nu = 75\text{m}^2\text{s}^{-1}$.

Figure 7a shows the initial cold bubble. Figures 7b and c depict the results at 900 seconds for fixed grid simulations with 300 meter and 33.3 meter resolution. The coarse grid simulation cannot capture the billows that form behind the gust front head. However, the general shape of the gravity current is well captured and, surprisingly, the gust front position is the same in both the coarse and fine resolution simulations. Generally, the propagation of the gust front is independent of the resolution though it does depend on the viscosity.

Adaptive simulation results are shown in Figs. 7d, e and f. In the adaptive simulations the refinement ratio is 3 and the truncation errors are computed and fine grids replaced every 25 coarser grid timesteps. Thus the fine grids are replaced every 100 seconds when one refinement level is used and, for two levels of refinement, the finest level grids are replaced every 33.3 seconds.

The adaptive simulation with a single level of refinement resolves the overall structure of the billows fairly well. There is still significant Gibbs phenomena associated with the propagating front and with the tail of the gravity current. The noise from the Gibbs phenomena is advected into the billows, particularly the leftmost billow. The adaptive simulation with two levels of refinement, where the finest grids have 33.3 meter resolution, compares well with the single fine grid run (compare Figs. 7c and f). The Gibbs phenomena are almost entirely removed and the position and shape of the billows are virtually identical in the two simulations. For most purposes the solutions are identical though there are small differences. For example, the middle billow in the fixed grid simulation has a slightly colder core than that in the adaptive simulation.

As noted, the finer grids are replaced periodically as the solution evolves. We include the adaptive solution at 600s to depict the changing grid structure over time. The finest level of grids is replaced 27 times over the course of this simulation. Also note that one of the finest grids is not placed on the lower boundary; fine grids can be placed anywhere in the solution domain. The solutions in the fine-grid overlap regions behave properly and the procedure of obtaining boundary values from the overlapping grid correctly resolves fine scale features passing through overlap regions. Also, the fine grids are not rotated in these simulations. We choose not to rotate the grids so as to always have gravity acting in a single coordinate direction. We will demonstrate fine-grid rotation in a 3-dimensional example.

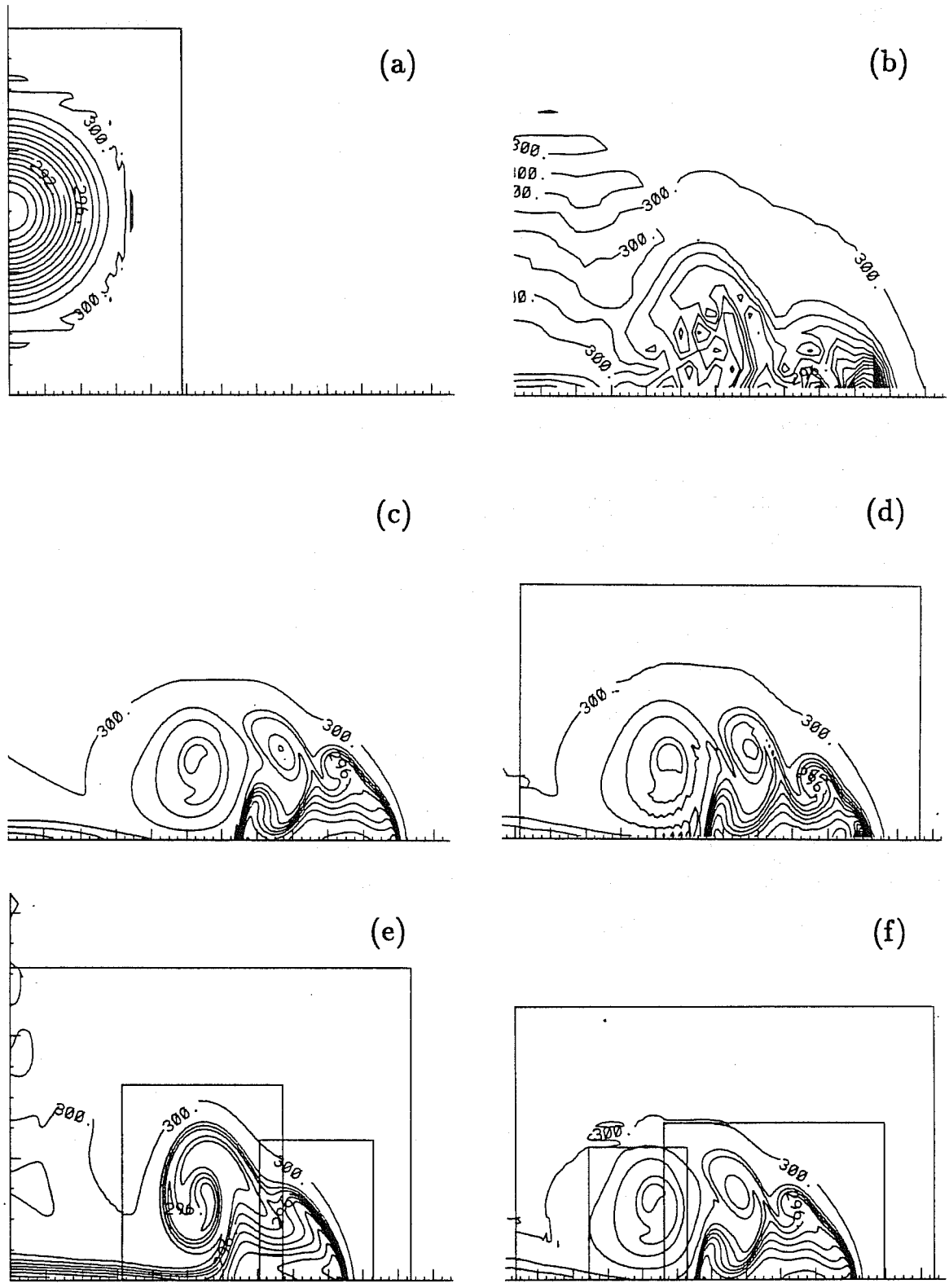

Figure 7 (a) Initial conditions for the cold bubble experiment, potential temperature with a contour interval of 1. The other panels show the potential temperature at 900s for (b) a single grid with $\Delta x = \Delta z = 300$m, (c) a single grid with $\Delta x = \Delta z = 33.3$m, (d) an adaptive run with one level of refinement with $\Delta x_f = \Delta z_f = 100$m, (e) an adaptive run with two levels of refinement with $\Delta x_f = \Delta z_f = 33.3$m at 600s and (f) the adaptive run with two levels of refinement at 900s.

Resolution (meters)	CPU time (seconds)	Memory (thousands of words)
300	5.1	$\sim$ 35
100	94.3	$\sim$ 300
33	2288	$\sim$ 920
300–100	35.3	$\sim$ 85
300–100–33	337.2	$\sim$ 170

Table 1 Timing and memory statistics for the 2-D cold-bubble simulation. Program instructions and miscellaneous memory are an additional 700×10^3 words. All computations performed on the NCAR CRAY Y-MP/864. The runtimes are with all plotting turned off.

We have demonstrated that the adaptive method can produce results almost identical to fixed grid results having the same resolution as the finest grid in the adaptive simulations. For the adaptive method to be cost effective, i.e., to actually justify its use, the CPU times and memory for the adaptive runs must be significantly less than that for the fixed grid runs. Table 1 presents the CPU times and approximate memory sizes for the adaptive and fixed grid codes. Obviously, increasing resolution increases both memory size and CPU times. Efficiency of the adaptive method is examined by comparing the 300-100 meter adaptive run with the fixed 100 meter grid run and comparing the 300-100-33.3 meter adaptive run with the fixed 33.3 meter grid run. With one level of refinement we decrease the CPU time (from the fixed grid run) by a factor of 3 and decrease the memory requirement by a factor of 3. Further refinement increases the efficiency. CPU times are decreased by almost a factor of 7 and memory requirements are reduced similarly.

Before considering the collapsing cold pool case, we emphasize that the AMR method is a local refinement method. The efficiency of the technique decreases as more area needs refinement. The break-even point for the method where the cost of an adaptive simulation will be approximately equivalent to a fixed grid simulation, occurs when around 50 to 60 percent of the coarse domain needs refinement at the finest refinement level. The AMR technique is suitable for local phenomena only.

The 2-D adaptive model has also been used for simulating a collapsing cold pool and resulting gravity current and the results are given in Skamarock and Klemp (1989). In these simulations the upper, lower and left boundary are solid, free-slip surfaces and the right boundary is open with boundary conditions specified as in Klemp and Wilhelmson 1978. The channel length is

40 km and the channel height is 10 km. The initial cold pool is specified as follows:

$$\theta = \begin{cases} 300 - \frac{5000-z}{5000}10 & z \leq 5000\text{m},\ x \leq 15000\text{m}; \\ 300 & \text{elsewhere.} \end{cases}$$

The initial velocities are zero and the initial pressure π is in hydrostatic balance with the temperature field. The model parameters used in the runs are $\Delta x_c = 250\text{m}$, $\Delta t_c = 3.0\text{s}$, $\Delta\tau = 0.5\text{s}$ and $\nu = \Delta x \cdot 1\text{m/s}$.

In these simulations the viscosity is now a function of the grid scale. We have chosen the viscosity such that only well resolved features are present on any grid. Figure 8 shows the solution for the collapsing cold pool at 900s in three different simulations. The first (Fig. 3A) is for a coarse grid run. No billows are present behind the head of the gravity current because the viscosity mixes out any incipient billows.

Comparing the fixed and adaptive grid runs with 27.8 meter resolution (Figs. 8b and c), it is immediately apparent that certain features in the solution are different. In particular, the leftmost eddy that appears in the adaptive solution depicted in Fig. 8b does not appear in the reference solution in Fig. 8c. Examination of the evolving adaptive solution shows that perturbations associated with changing resolutions were sufficient to initiate leftmost billow and the billow has sufficient truncation error associated with it to cause refinements to follow it. Even changes in the numerical scheme can produce perturbations that excite the billow. Evidence for this is provided by the simulations presented in Carpenter et al (1990), where a different numerical technique has been used to simulate the same problem and the leftmost eddy appears in their fine resolution simulation and yet does not appear in their coarse resolution results.

These results point out a difficulty in interpreting any simulations, particularly nested and adaptive simulations, when significant phenomena grow from infinitesimal perturbations – as is the case with Kelvin-Helmholtz billows. Numerical solutions will diverge as small perturbations are magnified and it is difficult to evaluate the accuracy of the solutions. Also problematic is the use of parameterizations that depend on the gridscale ($\Delta x\, \Delta t$), for example parameterizations of turbulence, convection, etc... There exists no exact solutions to these parameterized systems and it is difficult and often impossible to judge the accuracy of the numerical solutions. At the very least, grid-scale dependent parameterizations must be

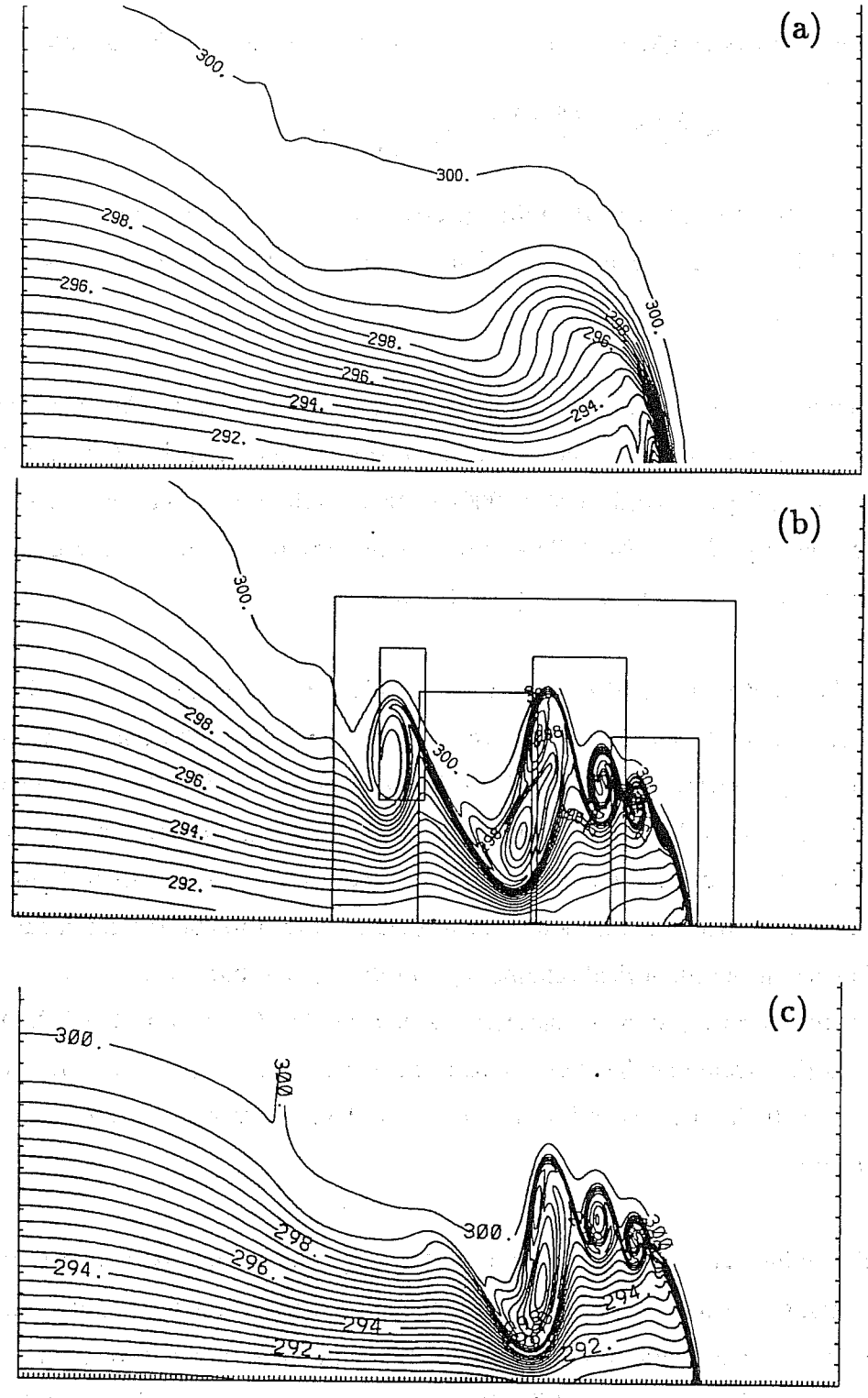

Figure 8 Collapsing cold pool simulation with potential temperature contoured at 0.5. (a) Single grid solution at 900s with $\Delta x = \Delta z = 250$m, (b) adaptive solution at 900s with two refinement levels, $\Delta x_f = \Delta z_f = 28.7$m and (c) single grid solution at 900s with $\Delta x = \Delta z = 28.7$m.

carefully examined when we ask that they function over a wide range of grid scales. The parameterizations may have a substantial impact in an evolving adaptive and nested solutions.

3.2.2 3-D Nonhydrostatic AMR Simulations

A three-dimensional model (constructed by Dale Durran) has been modified for use with the adaptive grid method. The model solves the full compressible equations of motion and is similar to the 2-D model described in Durran and Klemp (1983). An explicit time-split method is used to advance the elastic system of equations that includes both an acoustic filter based on divergence damping and a new technique for integrating the buoyancy equation (Skamarock and Klemp 1991a). The model includes terrain, moist processes (vapor, cloud and rain water) and is fully compressible. The 3-D model differs from Durran and Klemp's 2-D model primarily in the momentum equations and scalar equations for water substances; in the 3-D model they are cast in flux form whereas in the 2-D model they are in advective form. As in the 2-D model an equation for the pressure is used as opposed to computing with a continuity equation for ρ. The density is computed using a moist equation of state. Moist physics in this model are included through a Kessler parameterization scheme, calculated as described in Durran and Klemp using three forms of moisture; vapor, cloud and rain.

In its current implementation, the 3-D adaptive model does not perform automatic gridfitting. The user must periodically examine the evolving solution and input the positions of any new fine grids. In what follows, we show adaptive simulations of convective storms that demonstrate grid placement based primarily on an examination of low to mid-level updrafts, vorticity, rainwater and temperature gradients. With appropriate grid placement, these criteria appear sufficient for capturing isolated, strong convection. The simulations also demonstrate the robustness of the numerical methods used in the adaptive framework, particularly the boundary conditions between coarse and fine grids and between overlapping fine grids. A more complete description of the nonhydrostatic adaptive model can be found in Skamarock and Klemp (1991b).

We have adaptively simulated a squall line similar to the deep-shear case in Weisman *et al* (1988, see Section 4) where the environmental wind varies linearly from 0 ms^{-1} at the surface to 30 ms^{-1} at 5 km and remains 30 ms^{-1} above that. We initiate convection with a three-dimensional line thermal 200 km in length oriented at 45 degrees relative to the shear in a

1080 km square domain. In Weisman *et al*, the domain has an along line length of 120 km with periodic boundary conditions. Thus, we are no longer enforcing a particular line orientation (other than through the initial perturbation) and we now include squall-line end effects. The fine grids in the adaptive simulation and the Weisman *et al* single grid have 2 km horizontal resolution and 700 meter vertical resolution. In the adaptive simulation there are three levels of grids having 18, 6 and 2 km horizontal resolution. We use the domain speed in Weisman *et al.*

Figure 9a shows the flow field at $z = 3150$m at two hours for the adaptive run. The end cells are much stronger than any interior cells. By 4 hours, Figure 9b, the line has reoriented itself so that it is perpendicular to the shear. New convective cells are forming on the northern and southern ends of the line along the gust fronts propagating away from the storms that initially developed at the ends of the line.

As is evident in the solution at 2 and 4 hours, the line features pass smoothly through the overlapping grid boundary. The use of multiple, overlapping, rotated grids allows optimal resolution of the growing squall line, even as the line changes its orientation. A vertical cross section is given in Figure 10. Note that the cold pool has cleanly propagated through the western boundary, as have the upper-level storm-outflow features through the eastern boundary.

We conclude by noting that the adaptive model requires little additional memory over a single grid model other than that used to store the additional grids. In these simulations, the adaptive overhead is small, over 80 percent of the CPU time is used by the solver advancing the solution on a particular grid. The adaptive model allows us to resolve both the convection and the larger-scale flow economically, and in the case shown above, simple refinement criteria are sufficient for producing adequate simulations.

4. SUMMARY

Adaptive grid methods are advantageously used when phenomena needing refinement are local, i.e., they cover only a small portion of the solution domain. The adaptive methods can be grouped into two classes; global and local refinement techniques. While several methods are discussed in this paper, only two methods appear suitable for atmospheric calculations.

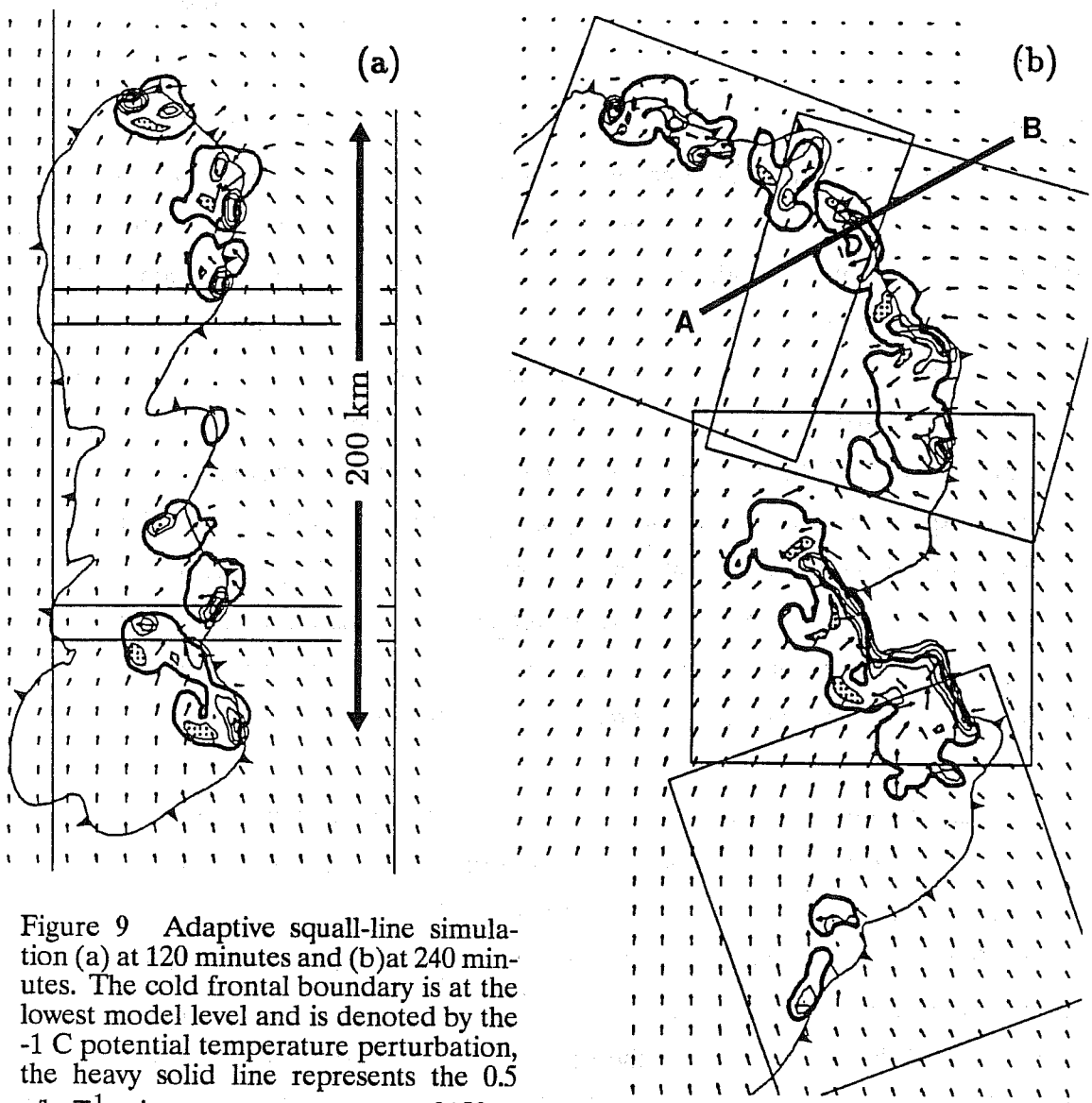

Figure 9 Adaptive squall-line simulation (a) at 120 minutes and (b)at 240 minutes. The cold frontal boundary is at the lowest model level and is denoted by the -1 C potential temperature perturbation, the heavy solid line represents the 0.5 g/kg^{-1} rainwater contour at z = 3150m. Vertical velocity is contoured at 5 ms^{-1} intervals with negative regions stippled The scale is the same in (a) and (b).

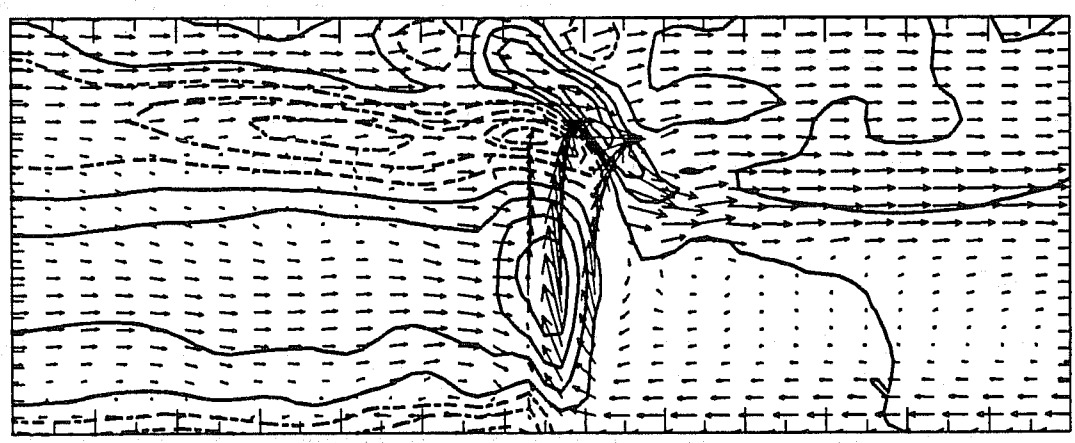

Figure 10 A vertical cross section through the squall line at four hours at AB in Figure 9b. The perturbation temperature field is contoured. Note that there are no anomalous disturbances at the various grid boundaries.

A global refinement technique has been used in atmospheric calculations by Dietachmeyer and Droegemeier (1991) and Dietachmeyer (1991). The method requires that the existing gridpoints move simultaneously with the integration of the equations. Thus the governing equations include terms for gridpoint movement. Gridpoint locations are recomputed each timestep by a grid generation algorithm which clusters points in regions needing refinement while also attempting to generate a smoothly varying grid. The method requires the transformation of the governing equations into curvilinear coordinates and the new coordinates may be non-orthogonal, hence many new terms arise in the new system. Grid generation can be very expensive, although the new grid generator introduced by Dietachmeyer (1991) appears to allow economical integrations of simple systems. While grid-generation methods still require research, a more pressing issue for the use of moving-gridpoint adaptive methods in atmospheric models is the formulation of parameterized physics on the nonuniform grids. This may be a major problem with parameterizations that depend on gridscale.

The local refinement technique of Berger and Oliger (1984) has been implemented in both hydrostatic models (Skamarock *et al*, 1989) and nonhydrostatic models (Skamarock and Klemp, 1989). The method makes use of multiple, overlapping fine grids to increase resolution where necessary. In this review we have presented results from the nonhydrostatic adaptive models. Two-dimensional simulations of gravity currents and three-dimensional simulations of severe convection (squall lines) demonstrate the applicability of the models. The work remaining in the application of this technique is the development of robust gridfitting algorithms. The three-dimensional model currently requires the user to specify the positions of any fine grids.

Both local and global refinement techniques can be used in atmospheric models. The AMR method of Berger and Oliger is more readily applicable because of its use of existing solvers. The method is being used in complex nonhydrostatic models for research purposes. The global refinement techniques for atmospheric models are still in the early stages of development.

REFERENCES

Anderson, D. A., 1983: Adaptive grid methods for partial differential equations. In *Advances in Grid Generation*, edited by K. N. Ghia and U. Ghia, AMSE, New York, NY.

Berger, M. and P. Colella, 1989: Local adaptive mesh refinement for shock hydrodynamics. *J. Comp. Phys.*, **82**, 64-84.

— and A. Jameson, 1985: Automatic adaptive grid refinement for the Euler equations. *AIAA Jour.*, **23**, 561-568.

— and J. Oliger, 1984: Adaptive mesh refinement for hyperbolic partial differential equations. *J. Comp. Phys.*, **53**, 484-512.

Brackbill, J. U., and J. S. Saltzman, 1982: Adaptive zoning for singular problems in two dimensions. *J. Comput. Phys.*, **46**, 342-368.

Caruso, S. C., J, H. Ferziger and J. Oliger, 1986: Adaptive grid techniques for elliptic flow problems. AIAA 24th Aerospace Sciences Meeting Paper AIAA-86-0498.

Clark, T. L., and R. D. Farley, 1984: Severe downslope windstorm calculations in two and three spatial dimensions using anelastic interactive grid nesting: A possible mechanism for gustiness. *J. Atmos. Sci.*, **41**, 329-350.

Carpenter, R. L., K. K. Droegemeier, P. R, Woodward, and C. E. Hane, 1990: Application of the piecewise parabolic method (PPM) to meteorological modeling. *Mon. Wea. Rev.*, **118**, 586-612.

Davies-Jones, R., 1985: Comments on "A kinematic analysis of frontogenesis associated with a nondivergent vortex". *J. Atmos. Sci.*, **42**, 2073-2075.

Dietachmeyer, G. S., 1991: On the application of continuous dynamic grid adaption techniques to meteorological modelling. Part II: Efficiency. Submitted to *Mon. Wea. Rev.*

— and K. K. Droegemeier, 1991: On the application of continuous dynamic grid adaption techniques to meteorological modelling. Part I: Basic formulation and accuracy. Submitted to *Mon. Wea. Rev.*

Durran, D. R. and J. B. Klemp, 1983: A compressible model for the simulation of moist mountain waves. *J. Atmos. Sci.*, **111**, 2341-2361.

Eiseman, P. R., 1987: *Comput. Meth. Appl. Mech. Eng.*, **64**, 321.

Gal-Chen, T. and R. Somerville, 1975: On the use of a coordinate transformation for the solution of the Navier-Stokes equations. *J. Comput. Phys.*, **17**, 209-228.

Hawken, D. F., J. J. Gottlieb and J. S. Hansen, 1991: Review of some adaptive node-movement techniques in finite-element and finite-difference solutions of partial differential equations. *J. Comput. Phys.*, **95**, 254-302.

Harrison, E. J., 1973: Three-dimensional numerical simulations of tropical systems utilizing nested finite grids. *J. Atmos. Sci.*, **30**, 1528-1543

Hoke, J. E., N. A. Phillips, G. J. DiMego, J. J. Tuccillo and J. G. Sela, 1989: The regional analysis and forecast system of the National Meteorological Center. *Wea. and Forecasting*, **4**, 323-334.

Jones, R. W., 1977: A nested grid for a three-dimensional model of a tropical cyclone. *J. Atmos. Sci.*, **34**, 1528-1553.

Kallinderis, Y. G., and J. R. Baron, 1989: Adaptation methods for a new Navier-Stokes algorithm. *AIAA Journal*, **27**, 37-43.

Klemp, J. B., and R. Wilhelmson, 1978: The simulation of three-dimensional convective storm dynamics. *J. Atmos. Sci.*, **35**, 78-106.

Perng, C. Y. 1990: Adaptive-Multigrid computations for incompressible flows, including geometry, temperature, and salinity effects. PhD Dissertation, Dept. of Mech. Engineering, Stanford Univ.

Skamarock, W. C. and J. B. Klemp, 1991a: On the stability of time-split numerical methods for the hydrostatic and nonhydrostatic-elastic equations. submitted to *Mon. Wea. Rev.*

– and J. B. Klemp, 1991b: Adaptive grid refinement for 2-D and 3-D nonhydrostatic atmospheric flow. *Mon. Wea. Rev.* to be submitted

—, J. Oliger and R. L. Street, 1989: Adaptive grid refinement for numerical weather prediction. *J. Comp. Phys.*, **80**, 27-60.

—, 1989: Truncation error estimates for refinement criteria in nested and adaptive models. *Mon. Wea. Rev.*, **117**, 882-886.

—, and J. B. Klemp, 1989: Adaptive models for 2-D and 3-D nonhydrostatic atmospheric flow. *Proc., 6th Int. Conf. on Numerical Methods in Laminar and Turbulent Flow*, Swansea, Wales, UK, 1413-1424.

Thompson, J. F., 1985: *Appl. Numer. Math*, **1**, 3.

Thompson, M. C., and J. F. Ferziger, 1989: AN adaptive multigrid technique for the incompressible Navier-Stokes equations, *J. Comp. Phys.*, **82**, 94-121.

Weisman, M. L., J. B. Klemp, and R. R. Rotunno, 1988: Structure and evolution of numerically simulated squall lines. *J. Atmos. Sci.*, **45**, 1990-2013.

Zhang, D.-L., H.-R. Chang, N. L. Seaman, T. T. Warner, and J. M. Fritsch, 1986: A two-way interactive nesting procedure with variable terrain resolution. *Mon. Wea. Rev.*, **114**, 1130-1139.